https://doi.org/10.1016/j.sab.2021.106105

Effect of spherical gold nanoparticles size on Nanoparticle enhanced Laser Induced Breakdown Spectroscopy

Zita Salajkova[1,2], Vincent Gardette[1], Jozef Kaiser[2], Marcella Dell'Aglio*[,3], Alessandro De Giacomo*[1,3],

[1.] University of Bari, Department of Chemistry, Via Orabona 4, 70126 Bari-Italy
[2.] Central European Institute of Technology (CEITEC), Brno University of Technology, Purkyňova 656/123, 612 00 Brno, Czech Republic
[3.] CNR-NANOTEC c/o University of Bari, Department of Chemistry, Via Orabona 4, 70126 Bari, Italy

Corresponding authors: Alessandro De Giacomo, email: alessandro.degiacomo@uniba.it

Marcella Dell'Aglio, email: marcella.dellaglio@cnr.it

Abstract

Recently the use of nanoparticles (NPs) for enhancing Laser ablation based analytical techniques, is getting a growing interest in analytical atomic spectroscopy. This technique is based on the deposition of NPs on the sample surface before the laser irradiation. The effect of the coupling of NPs plasmon with the laser pulse allows a notable improvement of the analytical signal. In this study, different sizes of spherical gold nanoparticles (AuNPs), 10 nm, 40 nm, 60 nm and 100 nm, have been employed to clarify the role of the NPs size on the signal enhancement during Laser Induced Breakdown Spectroscopy (LIBS). Therefore, a systematic investigation of the Nanoparticle Enhanced LIBS (NELIBS) have been done by varying the key experimental parameters as NPs surface concentration, laser fluence and laser spot size. The experimental results show that improvement of the emission signal during NELIBS occurs at specific NPs surface concentration and that this critical concentration depends on the NP size. When the concentration has been optimized for each NP size, the plasmon-enhanced ablation is moderately affected by the NPs size.

Keywords: NELIBS, LIBS, NPs size, surface concentration effects

1. Introduction

Recently the use of nanoparticles (NPs) for enhancing laser ablation based analytical techniques, such as Laser Induced Breakdown Spectroscopy (LIBS) [1] or Laser Ablation Inductively Coupled Plasma Mass Spectrometry (LA-ICP-MS) [2], is getting a growing interest in analytical atomic spectroscopy. In the case of LIBS, several experiments demonstrated that NPs deposition on the sample surface causes a huge enhancement of the emission signal and in turn allows the quantification at ppb levels with single-shot measurement [3]. Nanoparticle Enhanced LIBS (NELIBS) has been applied not only for traces determination, but also for decreasing the damage on the sample [4], or to increase the excitation of the plasma in fresh samples [5, 6]. The reasons of the emission signal enhancement have been ascribed to the plasmonic coupling between the NPs system and the incoming laser pulse but several aspects still need to be elucidated [7]. Previous experiments have shown that laser ablation mediated with NPs is notably different with respect to conventional laser ablation, but that the change

in the amount of ablated material is almost negligible [8-10]. In agreement with thermodynamics, the latter consideration means, that the total amount of energy spent for the ablation, in terms of ejected mass, is the same [7]. The most visible difference appears in the shape and topography of the laser induced crater on the sample when Nanoparticle Enhanced Ablation is enabled. In this case, holes of hundreds of nanometers are distributed on the crater surface [8-10]. The different distribution of the laser pulse energy on the sample when NPs have been deposited on the surface suggests a different ignition of the laser induced plasma and better atomization of the ejected mass [7,8].

Beyond the theoretical aspects of this intriguing phenomenon related to NPs mediated laser sampling, some practical issues should be pointed out in order to understand the most critical factors in the sample preparation and in the choice of NPs dimensions. One issue sometimes mentioned in literature is related to the effect of different spherical NPs size [6, 12-16]. In this paper we systematically investigated NELIBS on a metallic target namely titanium, varying the size of the spherical AuNPs from 10 nm to 100 nm as a function of the surface concentration, laser fluence and laser spot size.

This study clarifies that different NPs size does not affect notably the maximum signal enhancement, if optimal distances between the NPs are reached in order to have an efficient plasmon coupling. This observation also clarifies that the NPs comparison effect in NELIBS experiment should be done only after the NPs surface concentration has been optimized in order to set a suitable distance between the NPs. As different nanostructures require different spatial distribution, the effect of surface concentration on NELIBS enhancement must be investigated before comparing a different kind of nanostructures.

2. Materials and methods

2.1 Experimental set-up

The experiments were performed by using an Nd:YAG laser, Quantel Q-smart 850, with a pulse duration of 6 ns operating at 1064 nm with energies up to 615 mJ/pulse. During experiments, the laser energy variation was carried out by different flashlamp-Pockel cell delays (in the temporal range where the laser pulse's characteristics are negligibly affected). The spectrometer used was a Czerny-Turner (JY Triax 550) coupled with an ICCD (JY 3000) which was synchronized with the laser source by a pulse generator (Stanford DG 535) for performing emission spectroscopy of the plasma (Fig.S1).

The sample was placed perpendicularly to the laser beam, a 50 mm focal length lens, employed to focus the laser beam, was placed on a micrometric stage in order to change the laser spot size on the sample in a range from 0.6 mm up to 2.25 mm. The plasma emission was finally focused directly on the slit of the spectrometer by a set of biconvex lens. Different slit apertures have been employed in different experiments in order to avoid signal saturation during NELIBS and to allow a linear quantum efficiency of the detector when comparing LIBS and NELIBS. As discussed in a previous work [16], decreasing the slit and consequently the portion of detected plasma, NELIBS enhancement, although observable, is notably reduced.

LIBS and NELIBS spectra were acquired by employing one laser shot. The experiments consist in firing five laser pre-shots, the last of which is used to acquire the LIBS signal. Then NPs deposition is made on the formed LIBS crater and finally NELIBS is performed. Each experiment, repeated 4 times holding always the same conditions, has been performed on a fresh sample surface by moving the sample with a micrometric stage.

First, temporal evolution of the enhancement was investigated. Detector gate width was set at 100 ns and various delay, up to 5 μs, has been chosen to cover the whole plasma lifetime. Laser spot size was 2.2±0.2 mm and the laser pulse energy was 615 mJ (fluence = 16 J/cm^2). The monochromator slit was set to 100 μm. Employed AuNPs concentrations are reported in table 1.

Table 1 Au and AuNPs **c**oncentrations. Laser spot size 2.2±0.2 mm has been employed for the calculation of surface concentration. Different drop volumes of AuNPs colloidal solutions have been used to obtain a comparable surface concentration of Au-atoms after deposition on surface

AuNPs size (nm)	**Au mass concentration of mother solution (mg/ml)**	**AuNPs concentration of mother solution (n°AuNPs/ml)**	**Drop Volume (μl)**	**Au mass concentration for surface unit (mg/cm^2)**	**Number of AuNPs for surface unit (n°AuNPs/cm^2)**
10	0.06	5.94E+12	2.5	0.0039	3.91E+11
40	0.046	7.11E+10	3.5	0.0042	6.56E+9
60	0.043	1.97E+10	4.0	0.0045	2.08E+9
100	0.040	3.96E+09	4.0	0.0042	4.17E+8

Integrated measurements were performed in usual NELIBS conditions, with delay times of 0.3 μs and 1 μs and with a gate width of 5 μs. Laser spot size and pulse energy were 2.2±0.2 mm and 615 mJ (fluence =16 J/cm^2), respectively. The slit of the monochromator was 30 μm to avoid signal saturation.

Then, integrated measurements at different laser fluences have been performed with delay time of 1 μs, holding the same laser spot size (1.1±0.2 mm) and the same AuNPs surface concentration of table 1 by varying the employed drop volumes. Experiments at different laser spot sizes have been performed with delay time of 1 μs, holding the same laser fluence (16 J/cm^2) and the same AuNPs surface concentration of table 1 by varying the employed drop volumes. The employed monochromator slit apertures were 50 μm and 30 μm, respectively.

Experiments of NELIBS enhancements as a function of AuNPs concentration have been performed holding the laser energy at 615 mJ and the laser spot size at 2.2±0.2 mm (fluence =16 J/cm^2).

Finally, the standard deviations of the enhancement, the plasma temperature and the electron number density have been calculated by averaging the results obtained with four replica and are reported in the figures.

2.2 Sample preparation

Titanium target (Ti, 99.995% pure, 2.00" diameter x 0.250" thick, ± 0.010" all, K.J. Lesker) was utilized as a sample throughout the whole experiment. The employed NPs were gold nanoparticles colloidal solutions (stabilized suspensions in citrate buffer, OD1 from Sigma Aldrich) with four NP size namely 10±2 nm, 40±3 nm, 60±3 nm and 100±6 nm. In table 1 the Au mass concentration of the colloidal mother solution and the employed drop volume for each size are reported. The

corresponding number of AuNPs over the surface unit and the number of AuNPs/ml are also reported. In Fig. S4, the surface plasmon resonance spectra are reported for each employed AuNPs.

The solutions were deposited on the sample surface in the form of a drop, after 5 cleaning laser pre-shots. Due to the variation of surface hydrophobicity after pre-shots, the whole drop is contained, and consequently get dried, inside the pre-shots crater size. The drop was gently dried with airflow as described in [15]. The single laser shot employed for the NELIBS lead to a complete ablation of the dried drop. The volume of each solution was calculated to contain a comparable surface concentration of Au-atoms after deposition on a surface (the reason for this choice is explained in the next paragraph), resulting in 2.5 µl, 3.5 µl, 4 µl and 4 µl of 10 nm, 40 nm, 60 nm and 100 nm AuNPs mother solutions, respectively (see table 1).

3. Results and discussion

As mentioned in the introduction section, the most attracting aspect of NELIBS is the enhancement of the emission lines intensity with respect to LIBS, for this reason, the effect of different NPs size has been investigated measuring the enhancement calculated as the ratio between the NELIBS intensity on LIBS intensity [7, 15]. In Fig.S2 an example of the emission spectra acquired during these experiments is reported. Two representative Ti I (319.99 nm) and Ti II (311.76 nm) emission lines have been chosen to investigate the NELIBS enhancement. The spectroscopic data of the studied lines are reported in table S1.

In order to evaluate the intrinsic lack of uniformity of deposited layer of NPs, enhancement reproducibility has been investigated for each AuNPs size by employing 15 replica for each integrated measurement. The results and the standard deviations for the enhancement of Ti I and TiII emission peaks are therefore reported in Fig. S3.

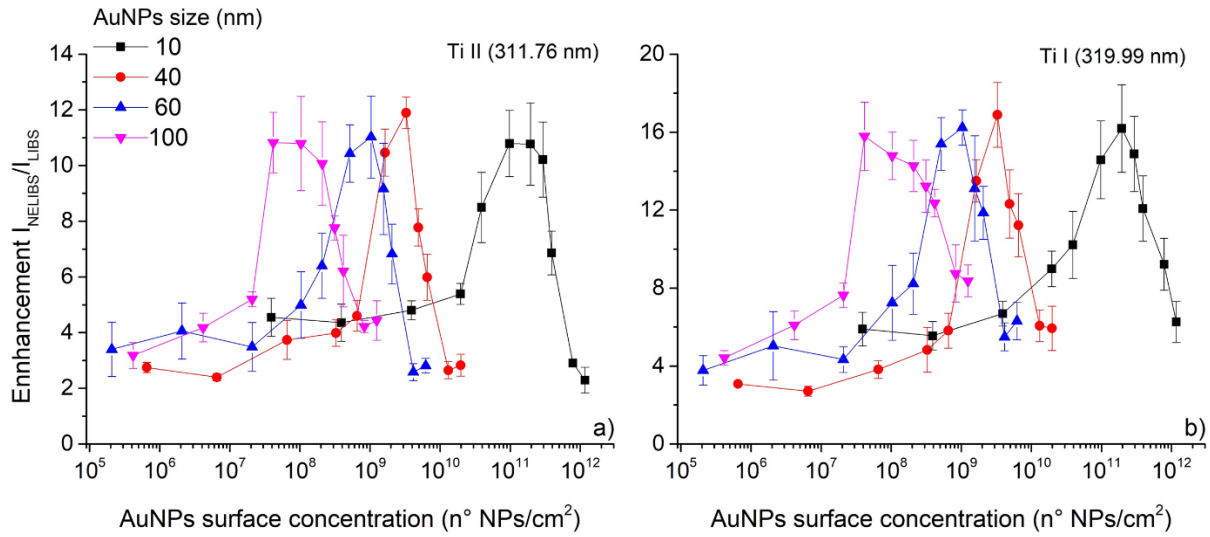

Fig.1 NELIBS enhancement as a function of the NP surface concentration (i.e the number of NPs for surface unit) of different NP sizes. Enhancement of a) Ti II (311.76 nm) and b) Ti I (319.99 nm) emission lines are shown. The error bar is the standard deviation.

In Fig.1 is reported the NELIBS enhancement as function of the NP surface concentration (i.e the number of NPs for surface unit) for different NP sizes and for both atomic and ionic transitions. It is possible to observe that the enhancement has the same general trend, consisting in the dramatic increase at the critical concentration, where plasmon coupling with the laser electromagnetic field occurs efficiently. Assuming that the NPs surface concentration establishes the average distance between the NPs since higher is the concentration on the surface closer are the NPs , when the distance between the NPs is similar or smaller than the NP size, the plasmon coupling with the laser pulse enables the electromagnetic field enhancement close to the sample surface and NELIBS signal increases [7]. Because with different NPs size, different distances are required to match the condition mentioned above, the maximum enhancement is obtained at lower NPs concentration for larger NPs. Moreover, the value of the intensity enhancement does not differ notably for NELIBS performed with different NPs size. The presence of the maximum enhancement corresponding to a range of concentration, rather than to a single value, suggests that, after a certain NPs concentration is reached, a further enhancement of the electromagnetic field due to shorter distances, does not improve the signal anymore. At too high surface concentration, tunnel effect between adjacent NPs, particle agglomeration and sample shielding occur and the enhancement decreases [15]. In other words, the main effect of the NPs size is that the smaller is the NPs, the higher is the surface concentration required for the signal enhancement. This is because smaller NP size requires smaller distance for exploiting the NELIBS effect. On the contrary, when NPs are larger, longer distances are required for coupling the plasmons, and in turn lower concentration is needed for the signal enhancement. For this reason, it has no sense to compare the effect of different NPs sizes keeping constant the surface concentration (in terms of number of NPs/cm^2), since the enhancement is dependent on the particles distances.

For the further experiments, AuNPs surface concentration was fixed for each AuNPs size to investigate the effect of the NPs size on the features of the NELIBS emission signal with respect to the LIBS one. The chosen concentration has a decreased enhancement after its maximum in order to avoid peak saturation. In these conditions the gold mass per surface unit was the same for all the NPs size, see table 1. In Fig S5, the enhancement at different NPs size as a function of surface concentration expressed as weight of gold deposited on the surface (mg/cm^2) is reported, just to put in evidence the overlapping of the enhancement curves and the chosen concentration of AuNPs for each size.

Fig.2 reports the temporal evolution of the plasma temperature (T) and of the electron number density (N_e) during NELIBS and LIBS, determined with Boltzmann plot and Stark broadening, respectively. In the table S1 the Ti II emission lines employed for the plasma temperature determination with the Boltzmann distribution are reported. The plasma electron number density has been determined with the Stark broadening of the Ti II emission peak at 311.98 nm [17].

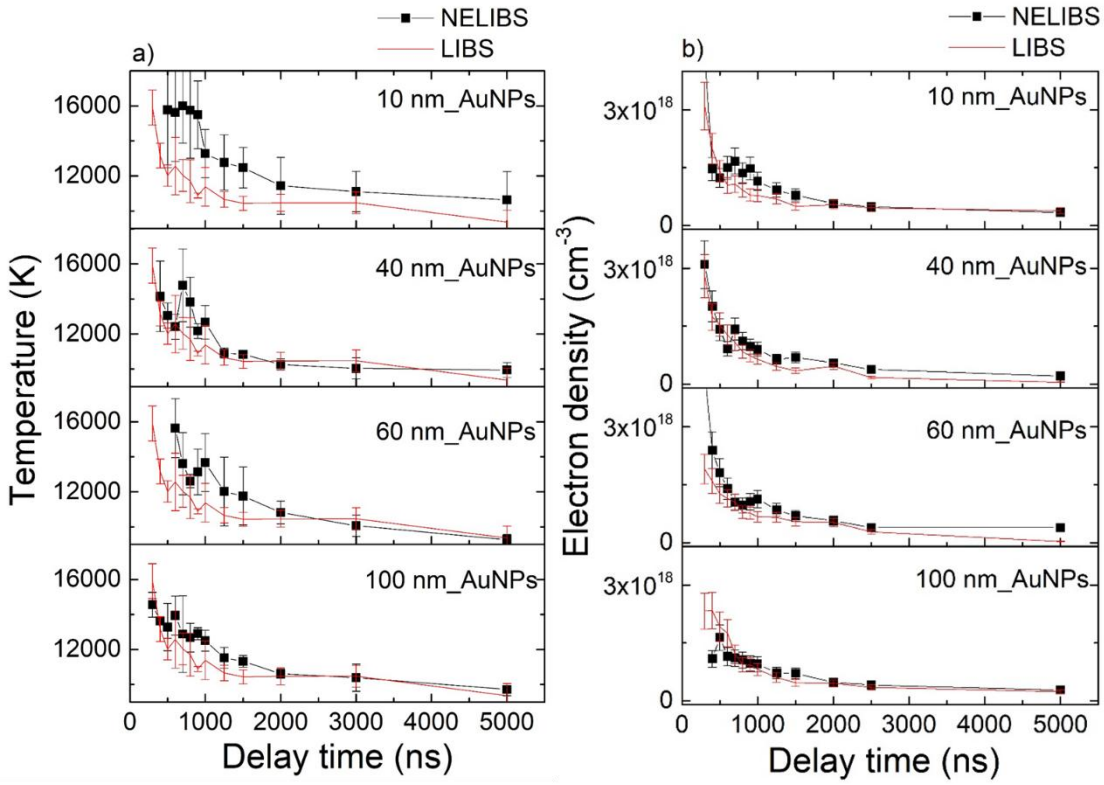

Fig.2 Temporal evolution of the plasma temperature (T) and of the electron number density (Ne) during LIBS and NELIBS with different AuNPs sizes. The error bar is the standard deviation.

It is interesting to note that the temperatures corresponding to NELIBS with different sizes of AuNPs are similar and they are slightly higher than the LIBS one. The negligible effect of the NP size on the plasma parameters, such as T and N_e, suggests that the main mechanisms of electron heating still depends on the photon energy [18], rather than the intensity of the electromagnetic field of the incoming radiation.

The temporal evolution of the enhancement of NELIBS with different sizes of AuNPs reveals that depending on the particle dimension, the maximum enhancement is reached at different delay time from the laser pulse as shown in Fig.3a. To investigate the NPs-plasma interaction during NELIBS with different NP's size, the emission signal of AuI at 312.28 nm is reported as function of time in Fig.3b. In this case, the maximum intensity is reached later for larger NPs as a consequence of the longer time required for vaporizing the entire NP [7].

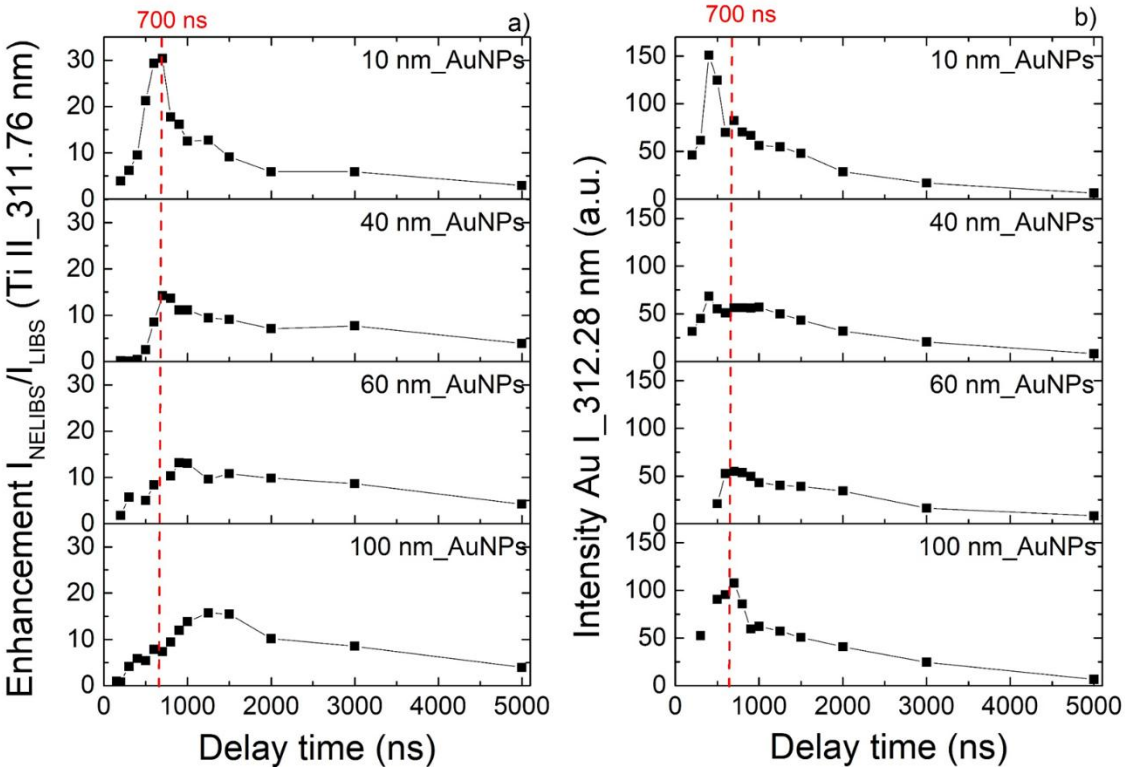

Fig.3 a) Temporal evolution of the Ti II (311.76 nm) emission line enhancement and of the b) emission intensity of Au I (312.28 nm) at different sizes of AuNPs

Inspecting Fig. 3a, 10 nm NELIBS has a sharp peak at 0.7 us, that gives an important contribution to the time-integrated enhancement reported in Fig.4, where a comparison between time-integrated measurements with delay times 0.3 μs and 1 μs are reported. It can be noted that, setting a detection delay time from the laser pulse of 1 us, the 10 nm NELIBS sharp peak at 0.7 μs is excluded and the enhancement does not seem to be affected by the NP size during NELIBS. On the contrary, the enhancements obtained when 0.3 μs delay time is used, are different at each AuNPs size and strictly linked to the different temporal evolution observed in Fig. 3a. It can be supposed that the AuNPs sizes can affect the dynamics of the ejection of material and consequently the plasma evolution. However, the time-integrated enhancement, over the whole plasma lifetime at 1 μs from the laser pulse, shows a negligible dependence on AuNPs size.

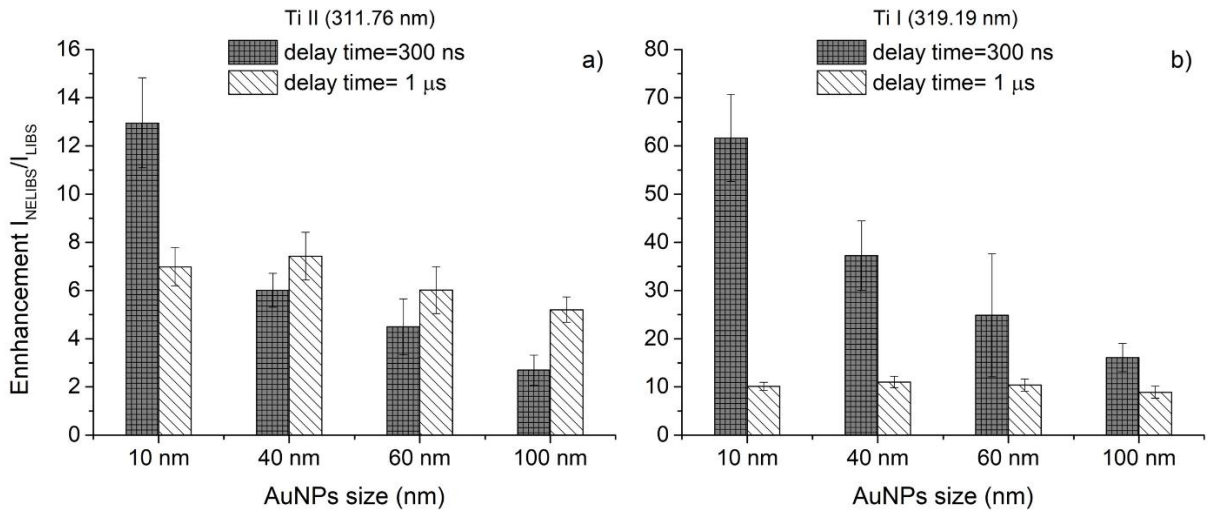

Fig.4 a) Ti II (311.76 nm) and b) Ti I (319.99 nm) emission lines enhancements obtained with integrated measurements employing two different delay times, 0.3 and 1 μs, gate width was 5 μs, the laser spot size was 2.2±0.2 mm. The error bar is the standard deviation.

These observations imply that there is a limit in enhancing the ablation efficiency in terms of atomization [7]. This limitation is caused by the amount of ablated mass. As it has been already reported in literature [7-10], the ablation mass is moderately affected by the deposition of NPs. Therefore, the enhancement, when NELIBS is at optimal condition, cannot increase limitless. As a matter of fact, when the NELIBS conditions are optimized, in order to increase further the enhancement, more ablated material is needed. To further investigate this effect, the dependence of the enhancement on the laser fluence is shown in Fig.5a and b. It can be noted that, in the investigated range of the energy, increasing the laser fluence, as more sample is ablated, the enhancement increases, regardless of the NPs size. The same trend of the enhancement, here as a function of the laser spot diameter, is observed in Fig.5c and d. In this case, although the laser fluence and the NPs concentration are kept constant, the enhancement clearly increases at larger spot diameter. This behaviour is also a result of greater ablated mass production. In this latter case it should be taken into account that for high ablated mass, a decreasing of the slope can be due to self-absorption.

Finally, these results show that the NELIBS enhancement is very sensitive to the experimental conditions and several parameters need to be taken into account when performing the NELIBS experiment. The most crucial question is to set the optimal surface concentration of NPs in order to have the maximum enhancement. The critical concentration, more than the average distances, include the intrinsic lack of uniformity that depends on the operating conditions and should be determined before every NELIBS experiment. Therefore, as the uniformity of the NPs deposition depends on the operating conditions [1], it is important to determine this surface concentration in every experiment.

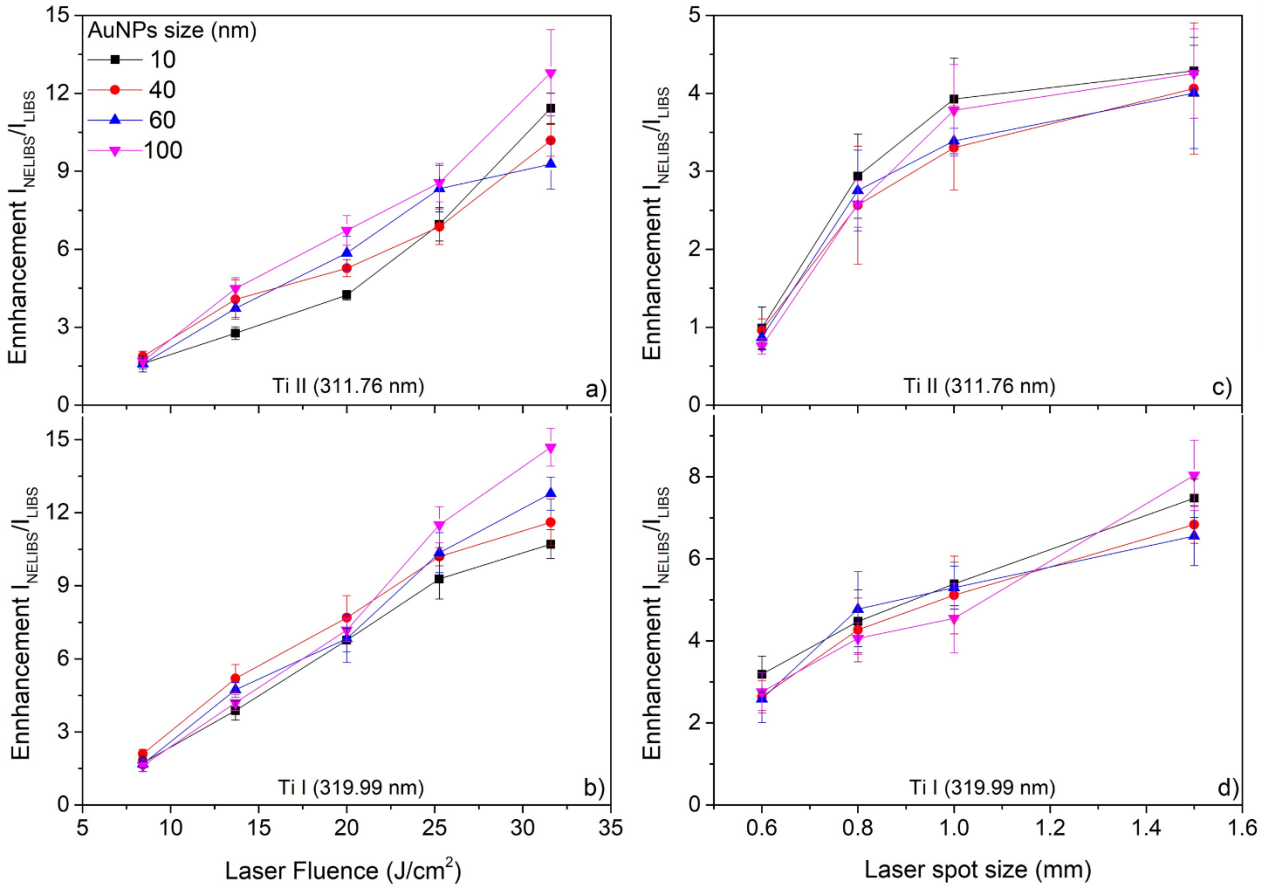

Fig.5 a) and c) Ti II (311.76 nm) and b) and d) Ti I (319.99 nm) emission lines enhancements as function of laser fluence (at fixed laser spot size 1.1±0.2 mm) and laser spot size (at fixed laser fluence 16 J/cm^2). Delay time = 1 μs, gate width=5 μs. The error bar is standard deviation.

4. Conclusion

In the present study, the effect of spherical AuNPs size on NELIBS enhancement has been discussed. Experimental results show that when optimal distances between the NPs dried on the sample is reached in order to have an efficient plasmon coupling with laser electromagnetic field, the different NPs size does not affect notably the maximum signal enhancement. It can be stated that a different NP size corresponds to a different optimal distance between NPs: larger is the NPs size, greater is the optimal distance and consequently, the required AuNPs surface concentration to obtain an efficient coupling, is lower. Therefore, when the surface concentration is beyond the critical one, the enhancement does not depend notably on the NP size. This suggests that the NELIBS enhancement process is limited by the ablated mass and that different kind of NPs size does not affect its quantity. Taking in mind this consideration, it is extremely important to know the optimal NPs concentration for a correct set up of the NELIBS experiment. The difference of signal enhancement that may be observed during NELIBS with different NP sizes, can be probably due to the different way the particles arrange in the deposition stage rather than to a different plasmonic effect. The latter consideration is related to the fact that when the plasmonic electromagnetic field grows above a critical value, the plasmonic system is weakened by electron tunneling and other aspects related to particles aggregation.

ASSOCIATED CONTENT

Supporting Information

Acknowledgements

This research is supported by MIUR PON RPASInAir ARS01_00820. Ms Zita Salajkova and Prof. Josef Kaiser would like to thank the Ministry of Education, Youth and Sports of the Czech Republic under the project CEITEC 2020 (LQ1601), CEITEC Nano Research Infrastructure (MEYS CR, 2016–2019) and CEITEC Nano+ project, ID CZ.02.1.01/0.0/0.0/16_013/0001728 that partially supported this research.

References

[1] Dell'Aglio, M., Alrifai, R., De Giacomo, A., Nanoparticle Enhanced Laser Induced Breakdown Spectroscopy (NELIBS), a first review (2018) Spectrochimica Acta - Part B Atomic Spectroscopy, 148, pp. 105-112.

[2] M. Holá, Z. Salajková, A. Hrdlička, P. Pořízka, K. Novotný, L. Čelko, P. Šperka, D. J. Novotný, P. Modlitbová, V. Kanický, J. Kaiser, Feasibility of Nanoparticle-Enhanced Laser Ablation Inductively Coupled Plasma Mass Spectrometry, Anal. Chem. 90 (20) (2018) 11820-11826

[3] De Giacomo, A., Koral, C., Valenza, G., Gaudiuso, R., Dellaglio, M., Nanoparticle Enhanced Laser-Induced Breakdown Spectroscopy for Microdrop Analysis at subppm Level (2016) Analytical Chemistry, 88 (10), pp. 5251-5257.

[4] Koral, C., Dell'Aglio, M., Gaudiuso, R., Alrifai, R., Torelli, M., De Giacomo, A., Nanoparticle-Enhanced Laser Induced Breakdown Spectroscopy for the noninvasive analysis of transparent samples and gemstones, (2018) Talanta, 182, pp. 253-258.

[5] Abdel-Salam, Z., Alexeree, S.M.I., Harith, M.A., Utilizing biosynthesized nano-enhanced laser-induced breakdown spectroscopy for proteins estimation in canned tuna (2018) Spectrochimica Acta - Part B Atomic Spectroscopy, 149, pp. 112-117.

[6] Zhao, X., Zhao, C., Du, X., Dong, D. Detecting and Mapping Harmful Chemicals in Fruit and Vegetables Using Nanoparticle-Enhanced Laser-Induced Breakdown Spectroscopy (2019) Scientific Reports, 9 (1), art. no. 906.

[7] De Giacomo, A., Alrifai, R., Gardette, V., Salajková, Z., Dell'Aglio, M., Nanoparticle enhanced laser ablation and consequent effects on laser induced plasma optical emission (2020) Spectrochimica Acta - Part B Atomic Spectroscopy, 166, art. no. 105794.

[8] Kiris, V.V., Tarasenko, N.V., Nevar, E.A., Nedelko, M.I., Ershov-Pavlov, E.A., Kuzmanović, M., Savović, J., Enhancement of Analytical Signal of Laser Induced Breakdown Spectroscopy by Deposition of Gold Nanoparticles on Analyzed Sample (2019) Journal of Applied Spectroscopy, 86 (5), pp. 900-907.

[9] Wang, M., Jiang, L., Wang, S., Guo, Q., Tian, F., Chu, Z., Zhang, J., Li, X., Lu, Y., Multiscale Visualization of Colloidal Particle Lens Array Mediated Plasma Dynamics for Dielectric

Nanoparticle Enhanced Femtosecond Laser-Induced Breakdown Spectroscopy (2019) Analytical Chemistry, 91 (15), pp. 9952-9961.

[10] Mangone, A., Mastrorocco, F., Giannossa, L.C., Comparelli, R., Dell'Aglio, M., De Giacomo, A., Nanoparticle enhanced laser ablation inductively coupled plasma mass spectrometry (2020) Spectrochimica Acta - Part B Atomic Spectroscopy, 163, art. no. 105731.

[11] Wu, K., Shen, J., Cao, D., Cheng, H., Sun, S., Hu, B., Coulombic Effect of Amphiphiles with Metal Nanoparticles on Laser-Induced Breakdown Spectroscopy Enhancement (2018) Journal of Physical Chemistry C, 122 (33), pp. 19133-19138.

[12] Zhang, L., Yang, Y., Optimally enhanced optical emission in laser-induced breakdown spectroscopy by combining a cylindrical cavity confinement and Au-Nanoparticles action (2020) Optik, 220, art. no. 165129.

[13] Shen, J., Wu, K., Cao, D., Wang, J., Hu, B., Effect of Ag nanoclusters deposited with magnetron sputtering on laser-induced breakdown spectroscopy enhancement (2019) Spectrochimica Acta - Part B Atomic Spectroscopy, 156, pp. 59-65.

[14] EL Sherbini, A.M., Parigger, C.G., Nano-material size dependent laser-plasma thresholds (2016) Spectrochimica Acta - Part B Atomic Spectroscopy, 124, pp. 79-81.

[15] De Giacomo, A., Gaudiuso, R., Koral, C., Dell'Aglio, M., De Pascale, O. Nanoparticle-enhanced laser-induced breakdown spectroscopy of metallic samples (2013) Analytical Chemistry, 85 (21), pp. 10180-10187.

[16] De Giacomo, A., Dell'Aglio, M., Gaudiuso, R., Koral, C., Valenza, G., Perspective on the use of nanoparticles to improve LIBS analytical performance: Nanoparticle enhanced laser induced breakdown spectroscopy (NELIBS) (2016) Journal of Analytical Atomic Spectrometry, 31 (8), pp. 1566-1573.

[17] J. Manrique, J. A. Aguilera, C. Aragon, Experimental Stark widths and shifts of Ti II spectral lines, Montly Noticy of the Royal Astronomical Society, 462, 1501–1507 (2016)

[18] Bogaerts, A., Chen, Z., Gijbels, R., Vertes, A., Laser ablation for analytical sampling: What can we learn from modeling? (2003) Spectrochimica Acta - Part B Atomic Spectroscopy, 58 (11), pp. 1867-1893.

For Table of Contents Only